Dalton Transactions

ROYAL SOCIETY OF CHEMISTRY

PAPER

View Article Online
View Journal | View Issue

Cite this: *Dalton Trans.*, 2026, **55**, 6008

Gold(I) dimers with hemilabile azophosphine ligands in catalysis

Emma J. Jordan, † Bethan L. Greene, † Laura E. English, Ellen M. Tait, Paul W. Davies * and Andrew R. Jupp *

Received 6th March 2026,
Accepted 25th March 2026

DOI: 10.1039/d6dt00553e

rsc.li/dalton

The first example of azophosphines acting as a bridging ligand between two metal centres is reported. The hemilability of the azophosphine ligand renders the gold(I) dimer formation reversible, so that the complex is not a catalytic dead-end. The catalytic ability of the gold(I) azophosphine complexes is demonstrated through a series of cyclisation reactions that form C–C and C–O bonds.

Introduction

Gold(I) catalysis has emerged as a versatile tool in modern synthetic chemistry, offering unique reactivity patterns that complement traditional transition metal catalysts.[1] The soft Lewis acidic nature of gold(I) complexes enables the efficient activation of π-systems such as alkynes, allenes, and alkenes, facilitating a wide array of transformations under mild conditions with high selectivity.[2] Alongside catalytic applications, Au(I) complexes of the type LAuX have applications in medicine,[3] as therapeutic and imaging agents,[4] and materials science.[5]

Active $[L–Au]^+$ cations are commonly generated *in situ* from L–Au–Cl precursors using AgX salts, however this approach can introduce problems from incomplete abstraction of chloride, light and moisture sensitivity, and the fact that the Ag(I) cation is not catalytically innocent.[6] As such, avoiding *in situ* catalyst activation is potentially advantageous and at minimum simplifies the experimental regime.[7] Although the LAuX motif only requires a monodentate ligand, bidentate ligands have found significant utility in gold chemistry, including bridging ligands for the formation of dimeric (dinuclear) gold complexes,[8] and in stabilising Au(III) centres for catalysis.[9] In catalysis, while the use of bidentate ligands that facilitate the irreversible formation of gold dimers from catalytically active $[L–Au]^+$ species would be deleterious, if such dimers can dissociate to an active monomeric form in solution then such species can be considered as stable pre-catalysts.

1,3-P,N ligands contain coordinating phosphorus and nitrogen centres linked by a single atom, typically carbon, and have many attractive properties as hybrid ligands, including cooperative effects, hemilability, and substrate activation for catalysis.[10] They present an interesting motif for gold(I) chemistry, and several dimeric complexes of the form $[\{Au(\mu P,N\text{-}L)\}_2]$ featuring head-to-tail 1,3-P,N ligands have been crystallographically characterised (Scheme 1A),[11] as have a range of analogous complexes with P,N ligands featuring longer linkers between the P and N atoms.[12] The 1,3-P,N ligands shown in Scheme 1A all feature the binding nitrogen atom in a heterocycle. **A** is a prototypical pyridyl phosphine,[11a] and only the coordination chemistry was probed. **B** is an imidazolyl phosphine, and the

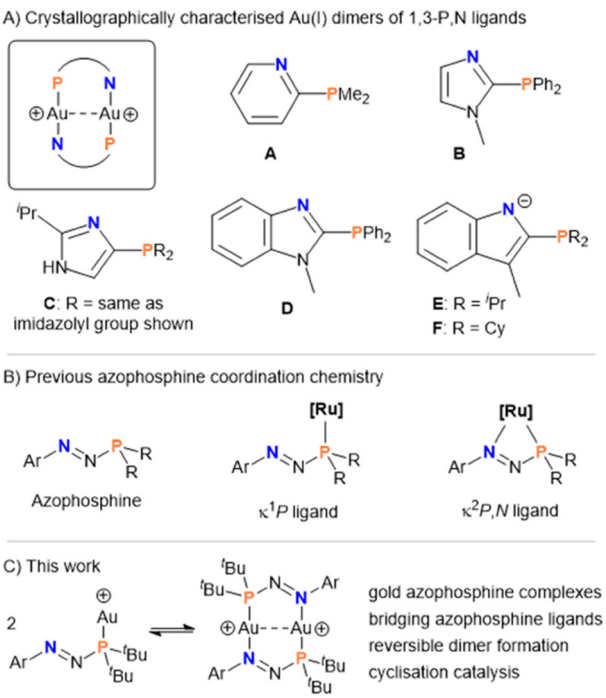

Scheme 1 A) Crystallographically characterised $[\{Au(\mu P,N\text{-}L)\}_2]$ complexes, where L is a 1,3-P,N ligand **A**–**F**. (B) General structure for azophosphine, and previous coordination modes observed in ruthenium complexes. (C) This work.

School of Chemistry, University of Birmingham, Edgbaston, Birmingham, B15 2TT, UK. E-mail: p.w.davies@bham.ac.uk, a.jupp@bham.ac.uk

† These authors contributed equally.

corresponding dimer displayed solid-state luminescence, and two different emission spectra observed depending on preparation conditions.[11b] The tris(imidazolyl) phosphine **C** forms the dimer with only one of the imidazolyl arms, and the complex showed promising anti-cancer properties,[11c] while the complex with benzimidazolyl phosphine ligand **D** displayed luminescent properties.[11d] **E** and **F** are phosphines bearing an anionic indole substituent which led to neutral dimers, but no further reactivity for these complexes was explored.[11e]

Azophosphines (ArN = N–PR_2; Scheme 1B) are heavier analogues of triazenes, and have recently emerged as precursors in the formation of phosphorus- and nitrogen-containing heterocycles.[13] We have also shown that azophosphines are a new class of 1,3-P,N ligand in which the central atom is a nitrogen.[14] A range of monodentate (κ^1P) and bidentate (κ^2P,N) ruthenium azophosphine complexes have been prepared (Scheme 1B), and the electronegative central N atom makes the ligand a relatively poor donor so the hemilabile ligands could promote transfer hydrogenation catalysis.[14b] To date the coordination chemistry of azophosphines has not been studied with metals other than ruthenium, and the potential utility of azophosphines as bridging ligands between multiple metal centres is unknown.

In this study we show that azophosphines can act as κ^1P ligands towards a gold(I) centre, and for the first time as $\mu P,N$ ligands between metal centres (Scheme 1C). The reversible nature of the dimer formation is probed, and we demonstrate that both the monomeric and dimeric complexes are catalytically competent in a range of cyclisation reactions that form C–O or C–C bonds.

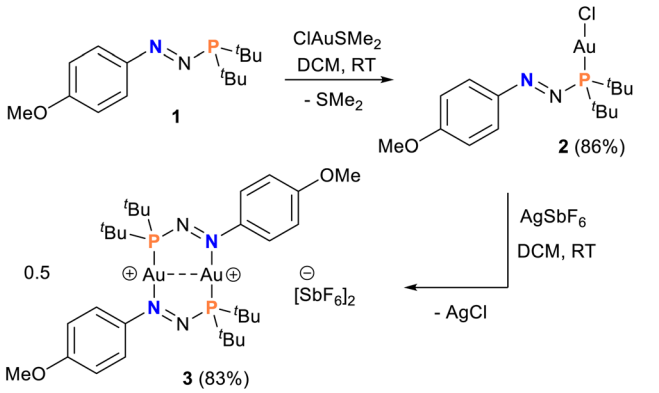

Scheme 2 Synthesis of gold azophosphine complexes **2** and **3** (with isolated yield).

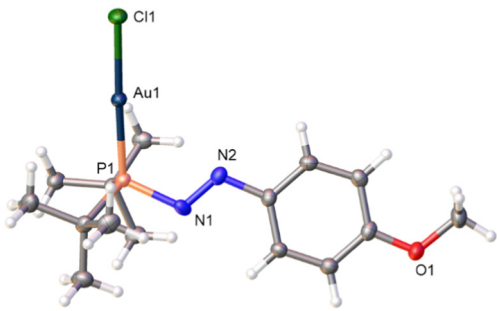

Fig. 1 Single crystal structure of Au(κ^1P-**1**)Cl (**2**). Thermal ellipsoids drawn at the 50% probability level. Selected bond distances (Å) and bond angles (°): Au1–P1 2.2354(10), Au1–Cl1 2.2970(9), P1–N1 1.728(3), N1–N2 1.261(4); P1–N1–N2 114.1(3), P1–Au1–Cl1 178.03(3).

Results and discussion

Synthesis and characterisation of gold(I) azophosphine complexes

Azophosphine (*p*-OMe)$C_6H_4N_2P(^tBu)_2$ (**1**) was prepared from a diazonium salt and a secondary phosphine borane adduct according to our previously published method.[14b] A dichloromethane solution of **1** was added to a stirring dichloromethane solution of $(Me_2S)AuCl$, resulting in the immediate formation of a red solution (Scheme 2). ^{31}P NMR spectroscopy showed quantitative conversion of the free azophosphine **1** at 111.7 ppm to a new species at 124.6 ppm. A similar downfield shift was previously observed in κ^1P coordination of azophosphines to ruthenium centres.[14] Removal of volatiles *in vacuo* isolated a vibrant red powder in 86% isolated yield. Red blocks of **2** suitable for single-crystal X-ray diffraction (Fig. 1) were grown by slow evaporation of a saturated dichloromethane solution of the product at room temperature, and showed the expected composition Au(κ^1P-**1**)Cl (**2**) with an almost linear P–Au–Cl bond angle of 178.03(3)°.[15] Monomer **2** exhibits no intermolecular Au···Au interactions, with the closest separation being over 7 Å in the extended crystal structure.

Reaction of complex **2** with one equivalent of $AgSbF_6$ led to formation of an orange solution and an orange precipitate; extraction of the product in excess dichloromethane yielded an orange solution and an off-white solid (AgCl) that could be separated by filtration. ^{31}P NMR spectroscopy of this dichloromethane solution revealed clean formation of a new resonance at 108.1 ppm. Removal of volatiles *in vacuo* afforded an orange solid in 83% isolated yield, and single crystals (orange blocks) could be grown by slow evaporation of a saturated dichloromethane solution. Single crystal X-ray diffraction studies confirmed the head-to-tail bridging nature of azophosphine **1** in the dimeric complex $[\{Au(\mu P,N\text{-}\mathbf{1})\}_2][SbF_6]_2$ (**3**) (Fig. 2).[15] Complex **3** crystallised in the monoclinic space group $P2_1/c$ with the Au–Au vector residing on a crystallographic inversion centre, rendering only half of the complex crystallographically unique.

Key bond metric data for complex **3** compared to the other crystallographically authenticated $[\{Au(\mu P,N\text{-}\mathbf{L})\}_2]$ dimers featuring 1,3-P,N ligands **A**–**F** are tabulated in Table 1.[11] All the previous P,N ligands in Table 1 feature a bridging carbon between the phosphorus and nitrogen centres, and the nitrogen is found within a heterocycle, whereas azophosphine **1** features an electronegative nitrogen bridging atom and the bonding nitrogen is acyclic. The Au–Au distance in **3** is 2.7782 (5) Å, which is statistically similar to the shortest Au–Au dis-

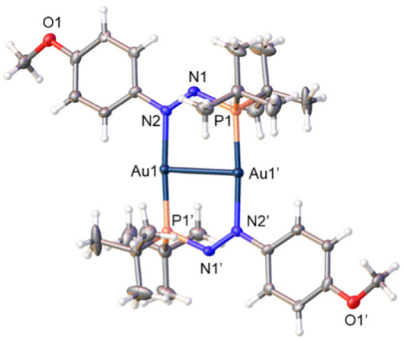

Fig. 2 Single crystal structure of $[\{Au(\mu P,N\text{-}\mathbf{1})\}_2]^{2+}$, the cationic component of **3**. The two SbF_6- counterions have been removed for clarity. Thermal ellipsoids drawn at the 50% probability level. Selected bond distances (Å) and bond angles (°): Au1–P1′ 2.2513(15), Au1–N2 2.123(5), P1–N1 1.741(5), N1–N2 1.276(7), Au–Au 2.7782(5); P1–N1–N2 121.8(4), P1′–Au1–N2 176.50(14).

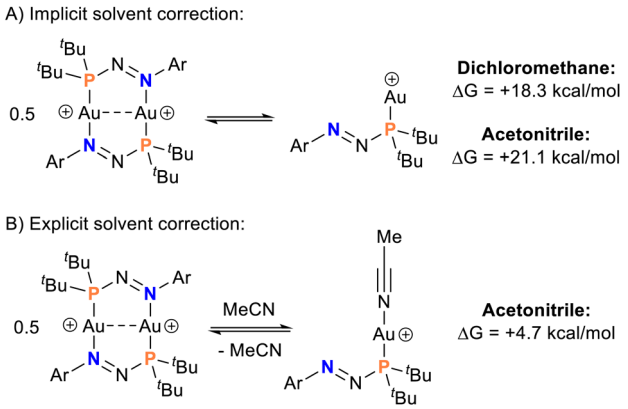

Scheme 3 Computational equilibria for gold(I) azophosphine monomers and dimers with (A) implicit and (B) explicit solvent corrections. Ar = (*p*-OMe)C_6H_4.

Table 1 Selected bond distances from crystallographically characterised $[\{Au(\mu P,N\text{-L})\}_2]$ dimers featuring 1,3-P,N ligands shown in Scheme 1

1,3-P,N ligand	Au–P (Å)	Au–N (Å)	Au–Au (Å)	Ref.
A	2.215(6)	2.086(16)	2.776(1)	11*a*
B	2.235(3)[a]	2.083(9)[a]	2.8174(10)[a]	11*b*
	2.238(3)[b]	2.090(11)[b]	2.8261(11)[b]	
C	2.245(4)	2.111(15)	2.8821(15)	11*c*
D	2.228(3)	2.074(4)	2.808(4)	11*d*
E	2.2586(15)	2.042(4)	2.8287(11)	11*e*
F	2.2526(7)	2.056(2)	2.8260(2)	11*e*
	2.2438(7)	2.040(2)	2.8278(3)	
	2.2521(7)	2.042(2)		
1	2.2513(15)	2.123(5)	2.7782(5)	This work

[a] BF_4^- counterions. [b] ClO_4^- counterions.

tance known for gold dimers featuring 1,3-P,N ligands, namely the (2-pyridyl)dimethylphosphine (2.776(1) Å),[11a] and is consistent with a significant aurophilic interaction.[16] The hexafluoroantimonate anions in **3** only weakly interact with the Au centres, with the shortest Au–F separation being 3.222 Å, comparable to the shortest Au–O separation of $[Au(midp)]_2^{2+}$ (midp = 1-methylimidazolediphenyl phosphine; entry 2 in Table 1) and its perchlorate anion (3.22(7) Å).[11b] The Au–N bond length in **3** of 2.123(5) Å is particularly long, which is consistent with this nitrogen centre being a relatively poor donor due to being adjacent to an electronegative nitrogen atom. This finding prompted us to explore the hemilability of this Au–N bond.

The equilibrium between the dication in **3**, $[\{Au(\mu P,N\text{-}\mathbf{1})\}_2]^{2+}$, and its monomeric cation, $[Au(\kappa^1 P\text{-}\mathbf{1})]^+$, was probed by density functional theory (DFT); see Experimental for full details. Using the polarisable continuum model (PCM) to implicitly model solvent effects, the dimer is significantly favoured by 18.3 kcal mol^{-1} and 21.1 kcal mol^{-1} in dichloromethane and acetonitrile, respectively (Scheme 3A). When the system was modelled explicitly using acetonitrile to coordinate to the gold cation in the monomeric form, the dimer is still favoured but only by 4.7 kcal mol^{-1} (Scheme 3B). These data suggest that in acetonitrile the monomeric form would be accessible at room temperature, and we theorised that the monomeric form might be similarly accessible in the presence of substrates that could coordinate to gold, and hence the hemilability of these ligands could enable catalysis.

To explore the nature of this equilibrium in acetonitrile experimentally, complex **3** was dissolved in acetonitrile and probed by NMR spectroscopy. The ^1H, $^{13}C\{^1H\}$ and ^{31}P NMR spectra for **3** in acetonitrile are all significantly different to those previously acquired in dichloromethane, consistent with a time-averaged signal for the monomer/dimer in the former. This difference is particularly apparent in the ^{31}P NMR spectra, with a $\Delta\delta$ of 18.1 ppm at room temperature ($\delta(^{31}P)$ = 108.1 in CD_2Cl_2, 126.2 in acetonitrile). Variable temperature ^{31}P NMR measurements of **3** in CD_3CN are also consistent with this equilibrium, with a downfield shift at higher temperatures (up to 60 °C), and an upfield shift at lower temperatures (down to −30 °C) (see Fig. 3). Notably, all single crystals grown from the acetonitrile solution that were tested were the previously described $[\{Au(\mu P,N\text{-}\mathbf{1})\}_2][SbF_6]_2$ dimers and not the acetonitrile adduct; this is consistent with the computational data that even though there is an equilibrium in acetonitrile,

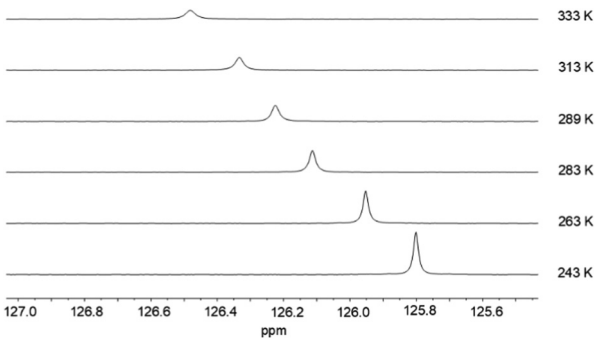

Fig. 3 Variable-temperature ^{31}P NMR spectra of a CD_3CN solution of **3**.

the dimer is still favoured. Complex **3** is stable as a solid for at least six months without any signs of decomposition.

Catalysis

The efficacy of the gold complexes as catalysts was explored through their application to several different transformations (Scheme 4). The azophosphine gold dimeric complex **3** was employed directly, whilst the gold(I) chloride complexes including **2** were activated using $AgSbF_6$ to maintain counter-ion consistency across each system. Loadings were maintained at 1 mol% of Au(I). The reactions were not forced to completion to enable a comparison of catalytic activity.

Direct alkyne hydrofunctionalisations were assessed through the cyclisation of propargylamide **4**[17] and propargyl ether **7**.[18] Heterocycles **5** and **8**, respectively, were formed in comparable yield when compared to a Ph_3PAuCl pre-catalyst.

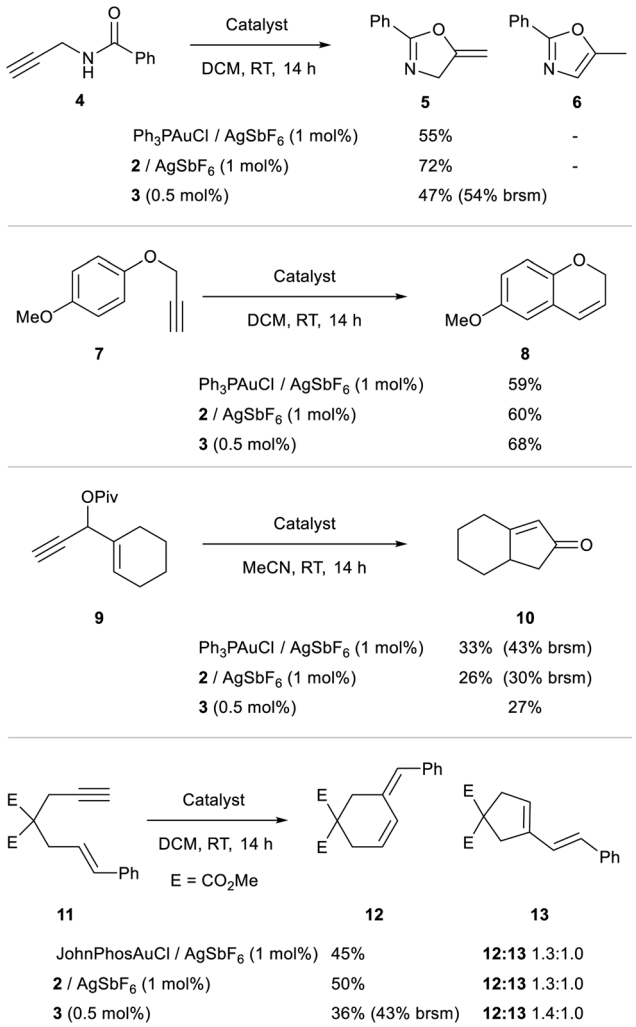

Scheme 4 Assessing the catalytic function of azophosphine gold complexes in typical gold-mediated transformations. Metal complexes added as freshly prepared stock solutions in the reaction solvent. Product yields and ratios reflect an average of two runs and were determined using ^1H NMR spectroscopy relative to an internal standard. brsm = based on recovered starting material.

None of the oxazole **6** from alkene-isomerisation was observed from reaction of **4**.

Similar efficacy was seen across the tested catalysis systems in the rearrangement-cyclisation of propargylic carboxylate **9** affording the bicyclic enone **10** after hydrolysis.[19] Despite the difference in ligand structure, cycloisomerisation of enyne **11**[20] afforded similar yields and ratios of diene isomers **12** and **13** using either JohnPhosAuCl or **2**, and slightly lower conversion was seen with the dimer **3**.

While the relative efficacy varied across reaction type, both **2** and **3** prove to be effective pre-catalysts leading to product formation and selectivities that broadly match those obtained with commonly used triphenylphosphine or JohnPhos Au(I) complexes under the same conditions.

Conclusions

We have shown that azophosphines can act as bridging ligands between two gold(I) centres for the first time, extending the known coordination chemistry of azophosphines beyond mononuclear ruthenium(II) complexes. The dicationic dimeric species exists in equilibrium with the monocationic monomer, which has been probed by variable temperature NMR spectroscopy and computational methods. The hemilability of the azophosphines ensures the dimer does not represent a catalytic dead-end, and indeed that the dimer can be used as a stable form of the activated catalyst species. The gold(I) azophosphine complexes have been used in a range of cyclisation reactions that form C–C and C–O bonds. In most cases the dimer gives similar activity to the gold(I) azophosphine chloride activated by silver salts *in situ*, demonstrating that the dimer can act as a stable self-activating pre-catalyst in these reactions.

Experimental

General considerations

Except as otherwise noted, the syntheses were performed using standard Schlenk line technique under a flow of dry, oxygen-free nitrogen, or an MBraun ECO glovebox under an atmosphere of dry, oxygen-free nitrogen with water and oxygen levels maintained at <0.1 ppm. Room temperature (RT) refers to reactions where no thermostatic control was applied and the temperature was recorded as 16–25 °C. Unless otherwise stated, overnight reactions refer to a period of 16 hours. All glassware and Teflon-coated stirrer bars were dried in an 80 °C oven overnight prior to use. All molecular sieves are 3 Å and purchased from VWR chemicals and were activated by heating at 400 °C under vacuum prior to use. Unless otherwise stated, degassing refers to three freeze–pump–thaw cycles. Me_2SAuCl,[21] azophosphine $(p\text{-OMe})C_6H_4N_2P(^t\text{Bu})_2$ (**1**),[14b] PPh_3AuCl[22] and catalysis substrates **4**,[23] **7**,[24] **9**[25] and **12**[19b] were prepared according to literature procedures. Details on solvents and instrument specifications can be found in the SI.

Synthetic procedures and characterisation

Synthesis of Au(κ^1*P*-(*p*-OMe)C$_6$H$_4$N$_2$P(^{t}Bu)$_2$)Cl (2). A solution of azophosphine **1** (102 mg, 0.36 mmol, 1 equiv.) in 2 mL DCM (dichloromethane) was added dropwise to a solution of Me_2SAuCl (106 mg, 0.36 mmol, 1 equiv.) in 4 mL DCM. The resulting red solution was stirred for three hours before removal of the volatiles *in vacuo* yielded **2** as a red solid (158 mg, 86%). Single crystals suitable for SCXRD were grown from slow evaporation of a saturated DCM solution at room temperature. ^{1}H (400.1 MHz, $CDCl_3$, 298 K): δ 7.86 (d, $^3J_{H-H}$ = 9 Hz, 2H; H_{Ar} (*p*-anisyl)), 7.01 (d, $^3J_{H-H}$ = 9 Hz, 2H; H_{Ar} (*p*-anisyl)), 3.92 (s, 3H; *p*-OCH_3), 1.42 (d, $^3J_{H-P}$ = 15 Hz, 18H; C(CH_3)$_3$). ^{13}C{^{1}H} (100.6 MHz, $CDCl_3$): δ 164.5 (s; *p*-C_{Ar} (*p*-anisyl)), 149.1 (d, $^3J_{C-P}$ = 43 Hz; *i*-C_{Ar} (*p*-anisyl)), 125.7 (s; CH_{Ar} (*p*-anisyl)), 114.6 (s; CH_{Ar} (*p*-anisyl)), 56.0 (s; *p*-OCH_3), 37.9 (d, $^1J_{C-P}$ = 27 Hz; *C*(CH$_3$)$_3$), 28.6 (d, $^2J_{C-P}$ = 4 Hz; C(*C*H$_3$)$_3$). ^{31}P{^{1}H} (161.7 MHz, $CDCl_3$): δ 124.6 (s). ^{31}P (161.7 MHz, $CDCl_3$): δ 124.9 (br. s). UV-Vis (DCM, nm) λ_{max}: 241 (m), 344 (s), 497 (w). ASAP-HRMS *m*/*z* for $C_{15}H_{25}ClN_2OPAu$ [M + H]$^+$: calcd (found) 516.1140 (516.1085), 515.1111 (515.1113), 514.1168 (514.1165), 513.1137 (513.1133). IR (cm^{-1}) ν_{max}: 2964 (w), 2922 (w), 2861 (w), 1597 (m, N=N), 1577 (m). Elemental Analysis: calcd (found) C% 35.14 (35.05), H% 4.91 (4.86), N% 5.46 (5.58).

Synthesis of [{Au(μ*P*,*N*-(*p*-OMe)C$_6$H$_4$N$_2$P(^{t}Bu)$_2$)}$_2$][SbF$_6$]$_2$ (3). A solution of complex **2** (23 mg, 0.04 mmol, 1 equiv.) in 2 mL DCM was added dropwise to a stirring solution of $AgSbF_6$ (13 mg, 0.04 mmol, 1 equiv.) in 2 mL DCM resulting in the immediate formation of an orange solution and precipitate. This solution was filtered through Celite, and the solid washed with DCM. The solvent was removed from the resulting orange solution *in vacuo* to yield **3** as an orange solid (25 mg, 83%). Single crystals suitable for SCXRD were grown from slow evaporation of a saturated DCM solution at room temperature. NMR spectroscopy data below are provided in CD_2Cl_2 and CD_3CN. ^{1}H (400.1 MHz, CD_2Cl_2, 298 K): δ 8.29 (d, $^3J_{H-H}$ = 9 Hz, 4H; H_{Ar} (*p*-anisyl)), 7.28 (d, $^3J_{H-H}$ = 9 Hz, 4H; H_{Ar} (*p*-anisyl)), 4.08 (s, 6H; *p*-OCH_3), 1.60 (d, $^3J_{H-P}$ = 18 Hz, 36H; C(CH_3)$_3$). ^{13}C{^{1}H} (100.6 MHz, CD_2Cl_2): δ 170.0 (s; *p*-C_{Ar} (*p*-anisyl)), 149.3 (d, $^3J_{C-P}$ = 26 Hz; *i*-C_{Ar} (*p*-anisyl)), 131.4 (s; CH_{Ar} (*p*-anisyl)), 117.8 (s; CH_{Ar} (*p*-anisyl)), 57.7 (s; *p*-OCH_3), 41.6 (d, $^1J_{C-P}$ = 24 Hz; *C*(CH$_3$)$_3$), 28.6 (d, $^2J_{C-P}$ = 5 Hz; C(*C*H$_3$)$_3$). ^{31}P{^{1}H} (161.7 MHz, CD_2Cl_2): δ 108.1 (s). ^{31}P (161.7 MHz, CD_2Cl_2): δ 108.1 (m). ^{1}H (400.1 MHz, CD_3CN, 298 K): δ 7.91 (d, $^3J_{H-H}$ = 9 Hz, 4H; H_{Ar} (*p*-anisyl)), 7.13 (d, $^3J_{H-H}$ = 9 Hz, 4H; H_{Ar} (*p*-anisyl)), 3.93 (s, 6H; *p*-OCH_3), 1.43 (d, $^3J_{H-P}$ = 16 Hz, 36H; C(CH_3)$_3$). ^{13}C{^{1}H} (100.6 MHz, CD_3CN): δ 166.3 (s; *p*-C_{Ar} (*p*-anisyl)), 150.2 (d, $^3J_{C-P}$ = 44 Hz; *i*-C_{Ar} (*p*-anisyl)), 126.9 (s; CH_{Ar} (*p*-anisyl)), 115.8 (s; CH_{Ar} (*p*-anisyl)), 56.9 (s; *p*-OCH_3), 38.6 (d, $^1J_{C-P}$ = 29 Hz; *C*(CH$_3$)$_3$), 28.4 (d, $^2J_{C-P}$ = 4 Hz; C(*C*H$_3$)$_3$). ^{31}P{^{1}H} (161.7 MHz, CD_3CN): δ 126.2 (s). UV-Vis (DCM, nm) λ_{max}: 237 (m), 354 (s), 422 (w). ESI-HRMS *m*/*z* for $C_{30}H_{50}N_4O_2P_2Au_2$ [M + Cl]$^+$: calcd (found) 992.2436 (992.2459), 991.2414 (991.2423), 990.2460 (990.2480), 989.2429 (989.2442). ESI-HRMS *m*/*z* for SbF_6 [M]$^-$: calcd (found) 236.8946 (236.8949), 234.8942 (234.8944). IR (cm^{-1}) ν_{max}: 2956 (w), 2926 (w), 2855 (w), 1601 (m, N=N), 1577 (m).

Computational details

DFT calculations were run with Gaussian 16 (C.01).[26] TPSS[27] optimizations including Grimme's D3 parameter set[28] were performed using the Def2TZVP basis set[29] with all stationary points being fully characterized *via* analytical frequency calculations as minima (all positive eigenvalues). Implicit solvation models were used to account for dichloromethane (ε = 8.93) and non-coordinated acetonitrile (ε = 35.688) using the polarizable continuum model (PCM).[30] Optimised coordinates and energies can be found in the SI.

Catalysis

For the cycloisomerisation reactions stock solutions of individual substrates **4** (0.2 M), **7** (0.2 M) and **9** (0.2 M), PPh_3AuCl (4 mM), **2** (4 mM), **3** (1 mM) and $AgSbF_6$ (4 mM) were prepared in CH_2Cl_2. For the hydrolytic cyclisation of **12** stock solutions of **12** (0.2 M), PPh_3AuCl (4 mM), **2** (4 mM), **3** (1 mM) and $AgSbF_6$ (4 mM) were prepared in CH_3CN.

Stock solutions of substrates (0.5 mL, 0.1 mmol) were added to a vial followed by stock solutions of the selected catalyst system [(a) PPh_3AuCl (0.25 mL, 1 μmol) then $AgSbF_6$ (0.25 mL, 1 μmol); (b) **2** (0.25 mL, 1 μmol) then $AgSbF_6$ (0.25 mL, 1 μmol); (c) **3** (0.5 mL, 0.5 μmol)] The vial was capped and the reaction stirred for 14 h at RT before being diluted with CH_2Cl_2 (2 mL) and passed through a pad of silica, eluting with CH_2Cl_2 (8 mL). The solvent was removed under reduced pressure. Product yield was determined by ^{1}H-NMR spectroscopy relative to an internal standard of 1,2,4,5-tetramethylbenzene and with comparison to the literature [Compounds: **5**,[23] **8**,[31] **10**,[19b] **12**,[20] **13** [25]]

Conflicts of interest

There are no conflicts to declare.

Data availability

Data for this article, including NMR spectra, IR spectra, UV-Vis spectra, mass spectra, and computational data are available at UBIRA at https://doi.org/10.25500/edata.bham.00001562.

Supplementary information (SI) is available. See DOI: https://doi.org/10.1039/d6dt00553e.

CCDC 2465037 (**3**) and 2465038 (**2**) contain the supplementary crystallographic data for this paper.[15a,b]

Acknowledgements

The authors thank the Royal Society (URF\R1\201636), the EPSRC (EP/W036908/1), and the University of Birmingham for funding. The computations described in this paper were performed using the University of Birmingham's BlueBEAR HPC

service; see https://www.birmingham.ac.uk/bear for more details.

References

1 (*a*) A. S. Hashmi and G. J. Hutchings, *Angew. Chem., Int. Ed.*, 2006, **45**, 7896–7936; (*b*) A. Fürstner and P. W. Davies, *Angew. Chem., Int. Ed.*, 2007, **46**, 3410–3449; (*c*) D. J. Gorin and F. D. Toste, *Nature*, 2007, **446**, 395–403.

2 (*a*) A. B. Gade, Urvashi and N. T. Patil, *Org. Chem. Front.*, 2024, **11**, 1858–1895; (*b*) M. Kumar, K. Kaliya and S. K. Maurya, *Org. Biomol. Chem.*, 2023, **21**, 3276–3295; (*c*) C. C. Chintawar, A. K. Yadav, A. Kumar, S. P. Sancheti and N. T. Patil, *Chem. Rev.*, 2021, **121**, 8478–8558; (*d*) D. Campeau, D. F. Leon Rayo, A. Mansour, K. Muratov and F. Gagosz, *Chem. Rev.*, 2021, **121**, 8756–8867.

3 M. E. Hoffmann and F. E. Kühn, *Chem. Soc. Rev.*, 2025, **54**, 10326–10343.

4 (*a*) E. E. Langdon-Jones and S. J. Pope, *Chem. Commun.*, 2014, **50**, 10343–10354; (*b*) A. S. Arojojoye and S. G. Awuah, *Coord. Chem. Rev.*, 2025, **522**, 216208.

5 M. Jin and H. Ito, *J. Photochem. Photobiol., C*, 2022, **51**, 100478.

6 D. Wang, R. Cai, S. Sharma, J. Jirak, S. K. Thummanapelli, N. G. Akhmedov, H. Zhang, X. Liu, J. L. Petersen and X. Shi, *J. Am. Chem. Soc.*, 2012, **134**, 9012–9019.

7 A. Franchino, M. Montesinos-Magraner and A. M. Echavarren, *Bull. Chem. Soc. Jpn.*, 2021, **94**, 1099–1117.

8 (*a*) T. A. C. A. Bayrakdar, T. Scattolin, X. Ma and S. P. Nolan, *Chem. Soc. Rev.*, 2020, **49**, 7044–7100; (*b*) W. Wang, C. L. Ji, K. Liu, C. G. Zhao, W. Li and J. Xie, *Chem. Soc. Rev.*, 2021, **50**, 1874–1912.

9 (*a*) A. Zeineddine, L. Estévez, S. Mallet-Ladeira, K. Miqueu, A. Amgoune and D. Bourissou, *Nat. Commun.*, 2017, **8**, 565; (*b*) K. Muratov, E. Zaripov, M. V. Berezovski and F. Gagosz, *J. Am. Chem. Soc.*, 2024, **146**, 3660–3674; (*c*) P. Font, H. Valdés and X. Ribas, *Angew. Chem., Int. Ed.*, 2024, **63**, e202405824; (*d*) V. W. Bhoyare, A. G. Tathe, A. Das, C. C. Chintawar and N. T. Patil, *Chem. Soc. Rev.*, 2021, **50**, 10422–10450; (*e*) R. Kumar and C. Nevado, *Angew. Chem., Int. Ed.*, 2017, **56**, 1994–2015.

10 (*a*) M. K. Rong, F. Holtrop, J. C. Slootweg and K. Lammertsma, *Coord. Chem. Rev.*, 2019, **380**, 1–16; (*b*) M. K. Rong, F. Holtrop, J. C. Slootweg and K. Lammertsma, *Coord. Chem. Rev.*, 2019, **382**, 57–68.

11 (*a*) Y. Inoguchi, B. Milewski-Mahrla and H. Schmidbaur, *Chem. Ber.*, 1982, **115**, 3085–3095; (*b*) V. J. Catalano and S. J. Horner, *Inorg. Chem.*, 2003, **42**, 8430–8438; (*c*) P. C. Kunz, M. U. Kassack, A. Hamacher and B. Spingler, *Dalton Trans.*, 2009, 7741–7747; (*d*) D. E. Jenkins and Z. Assefa, *J. Mol. Struct.*, 2017, **1133**, 374–383; (*e*) S. G. Rachor, R. Muller, P. Wittwer, M. Kaupp and T. Braun, *Inorg. Chem.*, 2022, **61**, 357–367.

12 (*a*) O. Crespo, E. J. Fernández, M. Gil, M. Concepción Gimeno, P. G. Jones, A. Laguna, J. M. López-de-Luzuriaga and M. Elena Olmos, *J. Chem. Soc., Dalton Trans.*, 2002, 1319–1326; (*b*) J. E. Aguado, M. C. Gimeno, A. Laguna and M. D. Villacampa, *Gold Bull.*, 2009, **42**, 302–309; (*c*) R. J. Bowen, J. Coates, E. M. Coyanis, D. Defayay, M. A. Fernandes, M. Layh and R. M. Moutloali, *Inorg. Chim. Acta*, 2009, **362**, 3172–3180; (*d*) S. Welsch, B. Nohra, E. V. Peresypkina, C. Lescop, M. Scheer and R. Reau, *Chem. – Eur. J.*, 2009, **15**, 4685–4703; (*e*) U. Siemeling, T. Klemann, C. Bruhn, J. Schulz and P. Štěpnička, *Z. Anorg. Allg. Chem.*, 2011, **637**, 1824–1833; (*f*) C. Voß, R. Pattacini and P. Braunstein, *C. R. Chim.*, 2011, **15**, 229–236; (*g*) R. Tan, F. S. N. Chiu, A. Hadzovic and D. Song, *Organometallics*, 2012, **31**, 2184–2192; (*h*) M. Bobin, I. J. Day, S. M. Roe and E. M. Viseux, *Dalton Trans.*, 2013, **42**, 6592–6602; (*i*) Z. Wang, Y. Wang and L. Zhang, *J. Am. Chem. Soc.*, 2014, **136**, 8887–8890; (*j*) K. Škoch, I. Císařová and P. Štěpnička, *Chem. – Eur. J.*, 2015, **21**, 15998–16004; (*k*) L. Zhang, W. Yu, C. Liu, Y. Xu, Z. Duan and F. Mathey, *Organometallics*, 2015, **34**, 5697–5702; (*l*) B. Michelet, D. Leboeuf, C. Bour, K. Škoch, F. Horký, P. Štěpnička and V. Gandon, *ChemPlusChem*, 2017, **82**, 442–448; (*m*) K. Škoch, I. Císařová and P. Štěpnička, *Chem. – Eur. J.*, 2018, **24**, 13788–13791; (*n*) O. Bárta, I. Císařová, J. Schulz and P. Štěpnička, *New J. Chem.*, 2019, **43**, 11258–11262; (*o*) A. C. Reiersolmoen, S. Battaglia, A. Orthaber, R. Lindh, M. Erdelyi and A. Fiksdahl, *Inorg. Chem.*, 2021, **60**, 2847–2855; (*p*) A. V. Artem'ev, A. Y. Baranov, A. S. Berezin, U. A. Lapteva, D. G. Samsonenko and I. Y. Bagryanskaya, *Chem. – Eur. J.*, 2022, **28**, e202201563; (*q*) F. Horký, M. Neubrand, I. Císařová, J. Schulz and P. Štěpnička, *ChemPlusChem*, 2023, **88**, e202300196; (*r*) Z. Leitner, I. Císařová and P. Štěpnička, *New J. Chem.*, 2023, **47**, 5930–5938.

13 (*a*) M. Y. Riu, W. J. Transue, J. M. Rall and C. C. Cummins, *J. Am. Chem. Soc.*, 2021, **143**, 7635–7640; (*b*) K. Tanaka, M. Y. Riu, B. Valladares and C. C. Cummins, *Inorg. Chem.*, 2022, **61**, 13662–13666; (*c*) E. D. E. Calder, L. Male and A. R. Jupp, *Dalton Trans.*, 2024, **53**, 15032–15039; (*d*) E. D. E. Calder, I. R. J. Hawes and A. R. Jupp, *Angew. Chem., Int. Ed.*, 2025, **64**, e202501421.

14 (*a*) E. J. Jordan, E. D. E. Calder, H. V. Adcock, L. Male, M. Nieger, J. C. Slootweg and A. R. Jupp, *Chem. – Eur. J.*, 2024, **30**, e202401358; (*b*) E. J. Jordan, E. D. E. Calder, B. L. Greene, H. V. Adcock, L. Male, P. W. Davies and A. R. Jupp, *Organometallics*, 2024, **43**, 2674–2685.

15 (*a*) CCDC 2465037: Experimental Crystal Structure Determination, 2026, DOI: 10.5517/ccdc.csd.cc2nr2bv; (*b*) CCDC 2465038: Experimental Crystal Structure Determination, 2026, DOI: 10.5517/ccdc.csd.cc2nr2cw.

16 H. Schmidbaur and A. Schier, *Chem. Soc. Rev.*, 2008, **37**, 1931–1951.

17 J. P. Weyrauch, A. S. Hashmi, A. Schuster, T. Hengst, S. Schetter, A. Littmann, M. Rudolph, M. Hamzic, J. Visus, F. Rominger, W. Frey and J. W. Bats, *Chem. – Eur. J.*, 2010, **16**, 956–963.

18 C. Nevado and A. M. Echavarren, *Chem. – Eur. J.*, 2005, **11**, 3155–3164.
19 (*a*) X. Shi, D. J. Gorin and F. D. Toste, *J. Am. Chem. Soc.*, 2005, **127**, 5802–5803; (*b*) C. Bürki, A. Whyte, S. Arndt, A. S. Hashmi and M. Lautens, *Org. Lett.*, 2016, **18**, 5058–5061.
20 C. Nieto-Oberhuber, M. P. Muñoz, S. López, E. Jiménez-Núñez, C. Nevado, E. Herrero-Gómez, M. Raducan and A. M. Echavarren, *Chem. – Eur. J.*, 2006, **12**, 1677–1693.
21 F. Sanchez-Cantalejo, J. D. Priest and P. W. Davies, *Chem. – Eur. J.*, 2018, **24**, 17215–17219.
22 D. Barik and R. S. Liu, *J. Org. Chem.*, 2022, **87**, 7097–7105.
23 S. Orbisaglia, B. Jacques, P. Braunstein, D. Hueber, P. Pale, A. Blanc and P. de Frémont, *Organometallics*, 2013, **32**, 4153–4164.
24 I. Volchkov and D. Lee, *J. Am. Chem. Soc.*, 2013, **135**, 5324–5327.
25 J. W. Faller and P. P. Fontaine, *J. Organomet. Chem.*, 2006, **691**, 1912–1918.
26 M. J. Frisch, G. W. Trucks, H. B. Schlegel, G. E. Scuseria, M. A. Robb, J. R. Cheeseman, G. Scalmani, V. Barone, G. A. Petersson, H. Nakatsuji, X. Li, M. Caricato, A. V. Marenich, J. Bloino, B. G. Janesko, R. Gomperts, B. Mennucci, H. P. Hratchian, J. V. Ortiz, A. F. Izmaylov, J. L. Sonnenberg, D. Williams-Young, F. Ding, F. Lipparini, F. Egidi, J. Goings, B. Peng, A. Petrone, T. Henderson, D. Ranasinghe, V. G. Zakrzewski, J. Gao, N. Rega, G. Zheng, W. Liang, M. Hada, M. Ehara, K. Toyota, R. Fukuda, J. Hasegawa, M. Ishida, T. Nakajima, Y. Honda, O. Kitao, H. Nakai, T. Vreven, K. Throssell, J. A. Montgomery Jr., J. E. Peralta, F. Ogliaro, M. J. Bearpark, J. J. Heyd, E. N. Brothers, K. N. Kudin, V. N. Staroverov, T. A. Keith, R. Kobayashi, J. Normand, K. Raghavachari, A. P. Rendell, J. C. Burant, S. S. Iyengar, J. Tomasi, M. Cossi, J. M. Millam, M. Klene, C. Adamo, R. Cammi, J. W. Ochterski, R. L. Martin, K. Morokuma, O. Farkas, J. B. Foresman and D. J. Fox, *Gaussian 16 Rev. C.01*, 2016.
27 (*a*) J. Tao, J. P. Perdew, V. N. Staroverov and G. E. Scuseria, *Phys. Rev. Lett.*, 2003, **91**, 146401; (*b*) K. P. Kepp, *J. Phys. Chem. A*, 2017, **121**, 2022–2034.
28 S. Grimme, J. Antony, S. Ehrlich and H. Krieg, *J. Chem. Phys.*, 2010, **132**, 154104.
29 F. Weigend and R. Ahlrichs, *Phys. Chem. Chem. Phys.*, 2005, **7**, 3297–3305.
30 J. Tomasi, B. Mennucci and R. Cammi, *Chem. Rev.*, 2005, **105**, 2999–3093.
31 T. Danelzik, S. Joseph, C. Mück-Lichtenfeld, C. G. Daniliuc and O. García Mancheño, *Org. Lett.*, 2022, **24**, 6105–6110.